One step toward a new generation of C-MOS compatible oxide PN junctions : structure of the LSMO/ZnO interface elucidated by an experimental and theoretical synergic work

One step toward a new generation of C-MOS compatible oxide p-n junctions: Structure of the LSMO/ZnO interface elucidated by an experimental and theoretical synergic work.

Daniele Pullini[§], Mauro Francesco Sgroi[§*], Agnes Mahmoud[§†], Nicolas Gauquelin[‡], Lorenzo Maschio[†], Anna Maria Ferrari†, Rik Groenen[×], Cas Damen[×], Guus Rijnders[×∞], Karel Hendrik Wouter van den Bos[‡], Sandra Van Aert[‡], Johan Verbeeck[‡].

[§]Centro Ricerche FIAT, Strada Torino 50, 10043 Orbassano, Torino (Italy)

[†]Dipartimento di Chimica, Università di Torino, via Giuria 5, I-10125 Torino (Italy), NIS (Nanostructured Interfaces and Surfaces) Centre, Università di Torino, via Giuria 5, I-10125 Torino (Italy)

[‡] EMAT University of Antwerp, Groenenborgerlaan 171, BE-2020 Antwerp, Belgium

[×] Twente Solid State Technology, Institutenweg 25 7521 PH ENSCHEDE, The Netherlands

[∞] Faculty of Science and Technology and MESA+ Institute for Nanotechnology, University of Twente, 7500 AE Enschede, The Netherlands

KEYWORDS: LSMO, ZnO, hetero-structure, first principle simulation, structural characterization

ABSTRACT: Heterostructures formed by $La_{0.7}Sr_{0.3}MnO_3$/ZnO (LSMO/ZnO) interfaces exhibit extremely interesting electronic properties making them promising candidatea for novel oxide p-n junctions with multifunctional features. In this work, the structure of the interface is studied through a combined experimental/theoretical approach, . Hetero-structures were grown epitaxially and homogeneously on 4" silicon wafers, characterized by advanced electron microscopy imaging and spectroscopy, and simulated by ab-initio DFT calculations. The simulation resultsuggest that the most stable interface configuration is composed by of the (001) face of LSMO, with LaO planes exposed, in contact with the (11 $\overline{2}$ 0) face of ZnO. The ab-initio predictions agree welly with experimental High Angle Annular Dark Field Scanning Transmission Electron Microscopy (HAADF-STEM) images and confirm the validity of the suggested structural model. Electron energy loss spectroscopy confirms the the atomic sharpness of the interface. From statistical parameter estimation theory, it has been found that the distances between interfacial planes are displaced from the respective ones of the bulk material. This can be ascribed to the strain induced by the mismatch between the lattices of the two materials employed.

Introduction

Complex oxide-based films and hetero-structures are at the core of next-generation nano-electronic, micro-electro-mechanical and macro-electronic devices expected to revolutionize fields of major social relevance as digital information and communication technologies, micro-actuation/micro-sensing and energy conversion. Such class of materials is characterized by an unprecedented wealth of functionalities, often being relevant to different fields of application, found in compounds that are extremely similar to each other in terms of chemistry, crystal structure and physical properties. One of the most promising hetero-structures which placed a milestone for the future development of oxide electronics is based on the LSMO/ZnO functional interface.

$La_{0.7}Sr_{0.3}MnO_3$ as a p-type perovskite semiconductor shows colossal magneto-resistance,[1] and its electrical and magnetic characteristics were proven to be strongly dependent on charge carrier concentration. $LaMnO_3$ is an antiferromagnetic insulator[2] while the Sr-substituted structure, being hole doped, undergoes metal–insulator and ferro-paramagnetic transitions at temperatures T_p and T_C, respectively, where the Curie temperature (T_C) is close to the peak temperature (T_p).[3] By changing the doping concentration, the electrical and magnetic properties of LSMO can be tuned to match the requirements of specific applications. An alternative method to control the carrier concentration is based on the modulation of the interfacial electronic band through the formation of a p-n hetero-junction using two dissimilar semiconductors with a significant lattice mismatch.[4]

ZnO under the normal conditions of deposition tends to be oxygen deficient exhibits a wide band-gap (3.37 eV) n-type semiconducting behavior. Nevertheless, the possibility to control its charge carrier concentration by changing the oxygen stoichiometry enables to tailor the bulk and interfacial electrical characteristics of the system.[5]

For above-mentioned reasons ZnO is an ideal candidate for being coupled to LSMO to obtain a p-n semiconducting junction: a thin depletion layer will be formed at the interface and the thickness of the layer and hence the carrier concentration in the system can be modulated by applying an external bias across the junction. Tiwari et al. fabricated the first LSMO/ZnO junction grown on a sapphire substrate.[6] This junction exhibited excellent rectifying behavior over the temperature range 20–300K. The electrical characteristics of the $La_{0.7}Sr_{0.3}MnO_3$ (LSMO) film in this heterostructure were found to be strongly modified by the built-in electric field at the junction. It was shown that by applying an external bias voltage, the thickness of the depletion layer, and hence, the junction resistance R_J can be finely tuned. An insulator-metal transition was observed for a bias voltage higher than 1 V.[6]

The junction showed also a photo-carrier injection effect that was explained as the generation of electron carriers due to the photo-excitation of the n-type semiconductor (ZnO)[7]. Hence light irradiation has been shown to control the electrical transport properties of LSMO by decreasing its holes concentration, due to the injection of electrons following the photo-excitation of ZnO. LSMO/ZnO junction showed rectifying and photo-excitation performances superior to those of the LSMO/Si junction[7] and for this reason the system is promising for various opto-electronic applications such as photo-detectors and photo-multipliers.

Moreover colossal magneto-resistance (CMR) in LSMO has attracted much attention not only for the study of the underlying physics but also for the exploration of potential applications. However, the practical utilization of the material has been limited by the required high magnetic fields (several Tesla).[8,9] In the past few years, the low-field magneto-resistance (LFMR) effect in LSMO has stimulated considerable interest since it constitutes a relatively large magneto-resistance effect in the low magnetic field (H <1 T) regime.[10] Tunable and enhanced low-field magneto-resistance (LFMR) was observed in epitaxial LSMO/ZnO self-assembled vertically aligned nano-composite (VAN) thin films.[11]

The LSMO/ZnO interface was studied by MacManus-Driscoll et al.[12] in vertical nano-composite hetero-epitaxial thin films prepared by pulsed laser deposition. The aim of that study was to demonstrate the possibility to control the strain coupling the two phases. They suggested a structural model of the strained interface based on Fourier-filtered images of high resolution TEM images along the interface boundary but their approach was not supported by theoretical modelling.

Despite these potential technological applications of the LSMO/ZnO junction, few studies were devoted to the theoretical understanding of the crystallographic and electronic structure of the interface between these two, structurally very different, oxides. Our study combined a computational approach based on ab-initio calculations with advanced electron microscopy imaging and spectroscopy to investigate the chemistry and real crystallographic structure of the LSMO/ZnO heterostructure at the atomic level. The theoretical modelling of the interface was used to guide and understand the fully epitaxial growth of this hetero-structure, and a modified pulsed laser deposition (PLD) allowed its fabrication for the first time on 4” silicon wafers with full conservation of the predicted stoichiometry and of the crystallographic orientation, features of paramount importance to obtain the desired functional properties (ferroelectric as well as ferromagnetic).

Silicon has been the most desirable platform for the integration of epitaxial multifunctional oxide devices with current semiconductor electronic devices for decades. The capability to grow high quality oxide layers on large area silicon substrates is therefore a major prerequisite for the integration of complex oxide ceramics into mainstream electronics. Not only are almost all electronics platforms silicon-based, but only silicon substrates are available with the necessary size, purity and electronic characteristics for commercial microelectronics semiconductor factories. Difficulties in coherent oxide growth are one of the biggest technological hurdles to oxide exploitation. The result of our study is a major milestone towards conceiving LSMO/ZnO p-n junctions compatible with CMOS technology, and accelerating the penetration of oxide electronics into the semiconductor marketplace.

Heterostructure growth

Sample fabrication is performed on a specially designed TSST PLD system which allows depositing on 4" wafers. Most importantly, in the design of the system most growth parameters can be set to values comparable to values in typical small scale PLD system experiments. With a 4" radiative heater, wafer growth temperatures of up to 900°C are achieved. The most significant difference in design compared to small scale systems concerns the challenge to grow homogeneously on this larger substrate size. The ablation plume is significantly smaller than the 4" wafer resulting in an inhomogeneous thickness profile when collected statically on substrates larger than 1". To obtain homogeneous films on larger substrates, the laser spot is scanned over the target, therefore spatially scanning the plume over the 4" wafer. While scanning the plume in lateral direction the heater rotates to ensure a full coverage of the plume over the full wafer.

These two extra parameters compared to small scale experiments, namely a plume scan curve and the heater rotation, are optimised to obtain a uniform thickness over the full wafer. In our experiments, plume scanning, wafer rotation in combination with laser repetition rate are set such that over the full wafer an average growth speed is obtained comparable with small scale experiments of 2nm/min with a thickness inhomogeneity less than 5% over the full wafer.

P-type doped (100) oriented 4" silicon wafers are used without any specific chemical surface treatment. To obtain an epitaxial relation between LSMO and silicon, a buffer layer stack[13] was deposited before the manganite (yttria-stabilized zirconia - YSZ, CeO_2 and $SrRuO_3$ – SRO). For the growth of both LSMO and ZnO, growth temperature, gas pressure, fluence, laser repetition rate, laser spot-size and target-to-substrate distance were set at respectively 800°C, 0.1mbar oxygen, 2.2J/cm^2, 20Hz, 2.5mm^2 and 55mm, with aimed film thicknesses of ~100nm for LSMO and 200nm for ZnO. In order to test device fabrication feasibility, not discussed any further in this work, patches of ZnO were grown using shadow masking by placing a wafer sized mask with 5x10mm holes directly on top of the wafer after growth of LSMO.

Structural characterisation and modelling of the LSMO-ZnO interface

The surface morphology of the full film was analysed by Scanning Electron Microscopy (SEM) and is shown in figure 1a. We can notice the presence of pillars with rather defined hexagonal shape with a diameter of ~100nm. A Cross sec-

tional sample in order to investigate the epitaxial quality of the different layers was prepared using the Focused ion Beam (FIB) technique. A low magnification STEM-HAADF image of the sample showing the full device structure and the good definition of the layers is presented in Figure 1b. In the following, only the top interface between LSMO and ZnO will be discussed. To further investigate the large scale structural properties of the sample, X-ray Diffraction (XRD) out-of-plane symmetrical scans were performed on a Panalytical X'Pert MRD diffractometer, and are shown in **Figure 1c**.

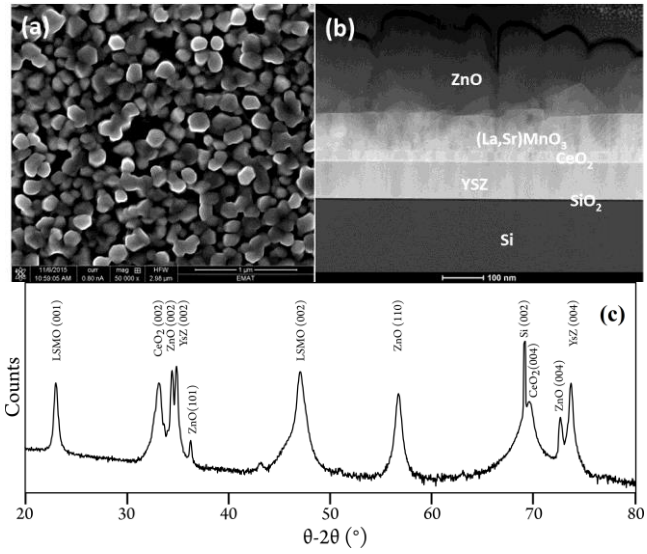

Figure 1: a) SEM image of the sample showing the hexagonal ZnO pillars. b) Cross sectional low magnification STEM-HAADF image of the sample showing the full device. c) XRD out-of-plane symmetrical scans. Clear out-of-plane single phase orientation is observed for the buffer layer stack and LSMO. ZnO is predominantly (0001) and $(11\overline{2}0)$ oriented.

Clear single phase out-of-plane c-axis orientation is observed for the YSZ, CeO_2 and LSMO layers, while the ZnO layer is mostly (001) and (110) oriented (using the Miller-Bravais notation these orientations correspond to (0001) and $(11\overline{2}0)$).

To investigate the crystalline quality of the structure more thoroughly, FWHM values of rocking curves around the 2-theta values of all films peaks were determined, with values all between 0.8° and 1.2°, indicating high crystallinity. It should be noted that the presented structural characterisation was performed on a specific position on the wafer, but represents the full structure over the full 4" wafer, indicating the potential of obtaining these high quality complex oxide stackings on larger areas and commercial substrates.

To examine the exact atomic structure of this LSMO/ZnO interface, cross-sectional samples have been analyzed by high resolution high angle annular dark field scanning transmission electron microscopy (HAADF-STEM) imaging, where contrast is proportional to the atomic number. This measurement has been performed in a Probe Corrected Scanning Transmission Electron Microscope (STEM) FEI Titan 80-300 microscope, operated at 300kV. Electron Energy Loss spectroscopy with 20ms dwell time per pixel and 0.25eV/pixel dispersion has been performed for chemical analysis on a Gatan GIF Quantum spectrometer.

Figure 2 presents the HAADF image of the LSMO-ZnO interface where the contrast is proportional to the atomic number (brightest columns are La/Sr). We can notice that the ZnO grows along the $[1\overline{1}00]$ direction whereas LSMO grows along the [001] direction. Image 2a presents a ZnO grain viewed along the [0001] zone axis and the grain in image 2b is seen along the $[11\overline{2}0]$ direction which are both present in the film and rotated by 90° respectively in the plane of the sample.

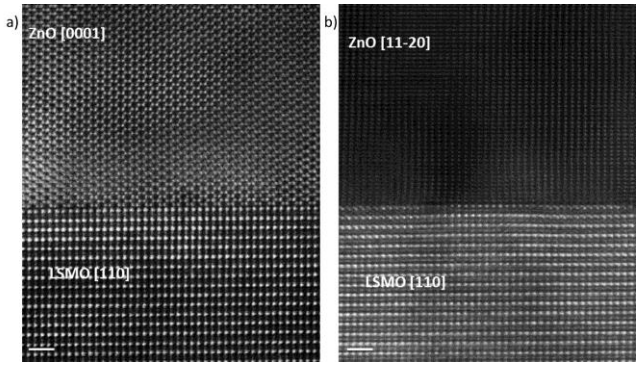

Figure 2: HAADF-STEM image of the LSMO/ZnO interface viewed along two different directions of the ZnO (a and b along [0001] and $[11\overline{2}0]$ axes respectively). Scale bar is 1 nm.

From atomically resolved EELS spectroscopy (presented in **Figure 3**), we can conclude that La(Sr)O is the termination layer of LSMO, an information complementary to the structural model proposed by MacManus-Driscoll et al.[12] and no inter-diffusion is present between the ZnO and the LSMO.

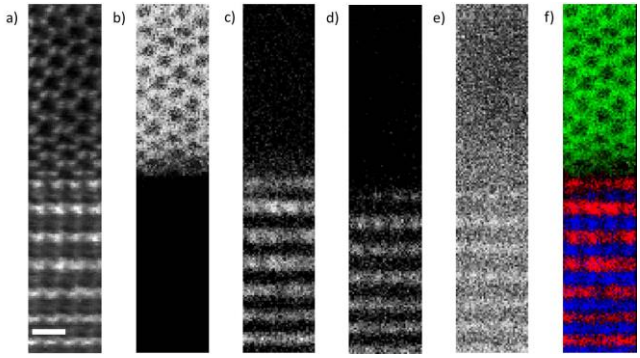

Figure 3: Atomic EELS mapping across the ZnO(top)/LSMO(bottom) interface with the HAADF image (a), the Zn $L_{2,3}$ (b), La $M_{4,5}$ (c), Mn $L_{2,3}$ (d) and O K (e) elemental maps and the RGB image (f) with Zn in green, La in red and Mn in blue showing the sharpness of the interface. Scale bar is 5Å.

Following the investigation carried out recently by some of us on the $LaMnO_3$/ZnO (LMO/ZnO) interface[14], we modelled the LSMO/ZnO interface by means of fully periodic ab-initio Density Functional Theory (DFT) simulations.

All the calculations reported in this manuscript were performed with the Crystal14 program for ab initio quantum chemistry of solid state[15,16]. In Crystal, the truncation of infinite lattice sums and as consequence the accuracy of the calculation is controlled by five thresholds T1; : : : ; T5; here T1 = T2 = T3 = 10^{-7} a.u., T4 = 10^{-8}, a.u. and T5 = 10^{-16} a.u. Reciprocal space was sampled according to a sub-lattice with shrinking factor 4, corresponding to 10 points in the irreducible Brillouin zone.

In the case of metallic systems, a Broyden[17] convergence accelerator and the smearing of the Fermi surface were adopted in order

to get rid of an extremely slow convergence and unphysical oscillations in the charge density during the spin-polarized SCF procedure. Equilibrium configurations were optimized by use of analytical energy gradients calculated with respect to atomic coordinates only.[18] A quasi-Newtonian technique was used, combined with the Broyden-Fletcher-Goldfarb-Shanno algorithm for Hessian updating.[19,20,21] The geometry optimization of the heterostructure was performed by means of density functional theory (DFT) at PBE level.[22] Lanthanium, manganese, strontium and zinc atoms were described by Hay-Wadt small-core pseudopotentials[23,24,25] with [3111-1]/(4sp/1d), [3111-41]/(4sp/2d), [2111-1]/(4sp/1d) and [4111-51]/(4sp/2d) additional Gaussian-type-functions (GFTs) for the valence electrons, respectively. Oxygen atom was described by triple-zeta valence [6211-411-1]/(4s/3p/1d) atom-centered GFTs. Hirshfeld's charge analysis[26] was performed by total energy calculations with PBE0[27] hybrid functional in combination with a triple-zeta valence all-electron basis set for all atoms. The structural model for LSMO was based on a 40-atom pseudo-cubic unit cell with no preservation of the cubic crystal symmetry, (with lattice parameters a = b = c). Similar structure models have been applied in former studies [28–31]. We also assumed that LSMO grows epitaxially on the buffer layer with cubic structure deposited on the silicon wafer. Due to the high spin state of Mn^{3+} (d^4 electron configuration), several magnetic arrangements are possible. In our case the ferromagnetic phase of LSMO was considered in the hetero-structure.

Taking ground from our previous results on the LMO/ZnO system, we verified that the most stable interface is composed by the (001) face of the pseudo-cubic LSMO, with LaO planes exposed, facing the (11 $\overline{2}$ 0) face of ZnO. Our estimate for the adhesion energy between the ZnO and LSMO layers in such interface is -132.3 meV/Å^3 (this value is corrected for basis-set superposition errors) by considering a 7-atomic plane thick LSMO slab and 4-atomic plane thick ZnO combined structure. This value contains a contribution of +6.3 meV/Å^3 embedded to the strain induced in the ZnO layer in order to match the two lattices at the atomic level[14]. The geometry optimized at the DFT level is reported in **Figure 4**. Statistical parameter estimation theory [32–34] was applied to a region of 10 unit cells width in both LSMO and ZnO to determine the atomic column positions and inter-planar distances. By averaging the individual column spacing in the growth direction over 10 values, the plane spacing was retrieved from the experimental images obtained with HAADF-STEM. These results were then compared to the DFT calculation results as presented on **Figure 5**. The bulk parts of LSMO and ZnO (more than 1nm away from the interface) have spacings 1.919 ± 0.011 Å and 1.613 ± 0.009 Å respectively which are identical to the reported bulk values [35,36]. Next to the interface we can notice a relaxation in a few steps: the first spacing between the interfacial ZnO and La(Sr)O planes is larger (2.15 ± 0.04 Å) but relaxes immediately to the bulk value of around 1.6 Å in the next plane; on the other hand, the first MnO_2 plane is shifted by around 0.2 Å towards the interface (1.77 ± 0.04 Å), the spacing between this MnO_2 plane and the next La(Sr)O plane on the other hand is the same as the bulk value already. The results are identical when considering both crystallographic directions from to different images of different areas of the film, increasing our confidence in these findings. Deviations from between experiment and DFT calculations for the outermost layers (part of the bulk) are due to the fact that these are terminating layers of the model (see **Figure 4**). So the results of the DFT simulations is in perfect agreement with the experimental structure obtained using HAADF-STEM.

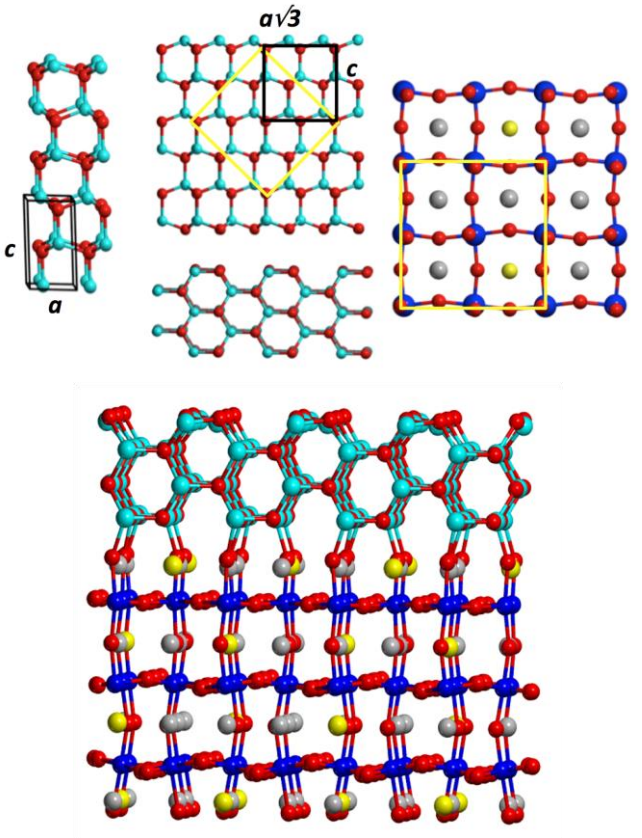

Figure 4: Top left: ZnO hexagonal bulk structure unit cell. Turquoise and red spheres denote Zn and O atoms respectively. Top center: ZnO (11 $\overline{2}$ 0) surface, in black the unit cell and yellow the coincidence cell with LSMO. Top right: LSMO (001) surface. In yellow the coincidence cell with ZnO. Red, blue, grey and yellow spheres are O, Mn, La and Sr respectively. Bottom: lateral view of the structural model of the interface used for the DFT calculations.

In order to pinpoint the origin of the atomic displacements at the interface, Mulliken's population analysis (which provides a means of estimating partial atomic charges from calculations carried out by computational chemistry [37]) was performed. In **Table 1** we report the atomic charges computed at the DFT(PBE0) level obtained with Mulliken's and Hirshfeld's population analysis. It can be seen that at the interface a mild charge transfer from the $La_{0.75}Sr_{0.25}O$ to the ZnO layer occurs. The two techniques yield different absolute values for the charges, but similar trends. In all cases, the small variations in charges from the "bulk" to the interface have negligible effects on the electrostatic potential at the interface and hence the observed displacements are unlikely to be ascribed to electrostatics.

The interfacial (La,Sr)O plane in the hetero-structure is shifted by 0.2 Å towards the first MnO2 plane (1.77 Å spacing), while the first ZnO plane is 2.15 Å away from the interface (normal spacing in ZnO is around 1.6 Å as discussed above). This structural change cannot be linked to strong electrostatic effects at the interface since the charge transfer between the LSMO and ZnO layers are negligible. The observed effect can likely be ascribed to the strain induced by the mismatch between the two materials' lattice parameters. Corrugation of the respective interface layers do accommodate the interfacial

strain leading to significant variations of the inter-planar distances.

Table 1: Computed average Mulliken and Hirshfeld (in parenthesis) charges on atoms, for "bulk" layers (in the middle of the slab) or interface layers as computed with a PBE0 hybrid functional.

	Zn	O	La	Sr	Mn
Bulk ZnO layer	1.43 (0.98)	-1.55 (-1.20)	-	-	-
Interface ZnO layer	1.38 (0.88)	-1.60 (-0.88)	-	-	-
Interface La_3SrO_4 layer	-	-1.60 (-1.60)	2.72 (2.93)	1.85 (2.05)	-
Bulk La_3SrO_4 layer	-	-1.40 (-1.30)	2.75 (3.02)	1.90 (2.08)	
Bulk MnO_2 layer	-	-1.45 (-1.45)	-	-	1.45 (1.20)

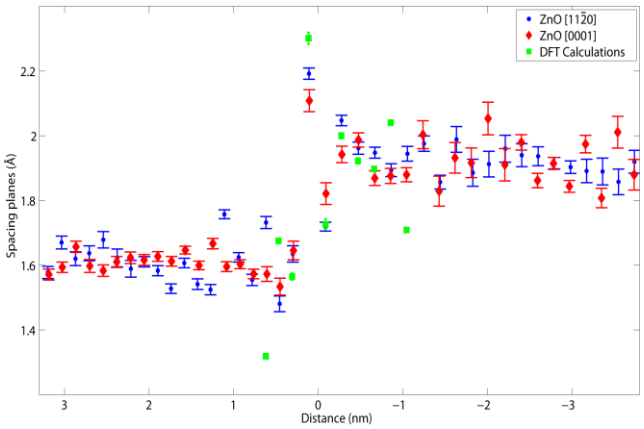

Figure 5: Results of the Gaussian fitting performed on the experimental HAADF images in the [11 $\bar{2}$ 0] and [0001] directions of the ZnO, the planes spacings in the ZnO is 1.613 ± 0.009 Å and for LSMO 1.919 ± 0.011 Å. These results match very well with the DFT presented in green. We can notice a relaxation next to the interface.

Conclusion

In this work we have clearly and unambiguously characterized the structure of the LSMO/ZnO interface, on high-quality samples as synthesized by means of pulsed laser deposition. Thanks to a cross-confirmation between DFT calculation and STEM measurements, we were able to verify that some mild structure distortions appear at the interface with respect to the bulk, which however seem not to affect significantly the electronic structure and atomic local charges of Zn and O. This latter aspect is significant in view of potential applications of the hetero-structure in electronic devices.

AUTHOR INFORMATION

Corresponding Author

*mauro.sgroi@crf.it

ACKNOWLEDGMENT

Financial support is acknowledged from the European Commission - DG research and innovation to the collaborative research project named Interfacing oxides (IFOX, Contract No. NMP3-LA-2010-246102). N.G. and J.V. acknowledge the European Union (EU) Council under the 7th Framework Program (FP7) ERC Starting Grant 278510 VORTEX for support. S.V.A. and K.H.W.B. acknowledge financial support from the Research Foundation Flanders through project fundings (G.0374.13N , G.0368.15N, and G.0369.15N) and a Ph.D. research grant to K.H.W.B. The microscope was partly funded by the Hercules Fund from the Flemish Government. The microscope used in this work was partly funded by the Hercules Fund from the Flemish Government. CINECA is acknowledged for computational facilities (Iscra project HP10CMO1UP).

ABBREVIATIONS

PLD pulsed laser deposition; XRD X-ray Diffraction; EELS electron energy loss spectroscopy; HAADF-STEM high angle annular dark field scanning transmission electron microscopy; SEM scanning electron microscopy; DFT density functional theory; YSZ yttria-stabilized zirconia.

REFERENCES

(1) Ramirez, A. P. Colossal Magnetoresistance. *J. Phys. Condens. Matter* **1997**, *9* (39), 8171–8199.

(2) Von Helmolt, R.; Wecker, J.; Holzapfel, B.; Schultz, L.; Samwer, K. Giant Negative Magnetoresistance in Perovskitelike La2/3Ba1/3MnOx Ferromagnetic Films. *Phys. Rev. Lett.* **1993**, *71* (14), 2331–2333.

(3) Granger, P.; Pârvulescu, V. I.; Kaliaguine, S.; Prellier, W. *Perovskites and Related Mixed Oxides: Concepts and Applications*; 2016.

(4) Katsu, H.; Tanaka, H.; Kawai, T. Photocarrier Injection Effect on Double Exchange Ferromagnetism in (La, Sr)MnO3/SrTiO3 Heterostructure. *Appl. Phys. Lett.* **2000**, *76* (22), 3245.

(5) Tamvakos, A.; Calestani, D.; Tamvakos, D.; Mosca, R.; Pullini, D.; Pruna, A. Effect of Grain-Size on the Ethanol Vapor Sensing Properties of Room-Temperature Sputtered ZnO Thin Films. *Microchim. Acta* **2015**, *182* (11–12), 1991–1999.

(6) Tiwari, A.; Jin, C.; Kumar, D.; Narayan, J. Rectifying Electrical Characteristics of La0.7Sr0.3MnO3/ZnO Heterostructure. *Appl. Phys. Lett.* **2003**, *83* (9), 1773.

(7) Lord, K.; Hunter, D.; Williams, T. M.; Pradhan, A. K. Photocarrier Injection Effect and P-N Junction Characteristics of La0.7Sr0.3MnO3/ZnO and Si Heterostructures. *Appl. Phys. Lett.* **2006**, *89* (5), 52116.

(8) Jin, S.; Tiefel, T. H.; McCormack, M.; Fastnacht, R. A.; Ramesh, R.; Chen, L. H. Thousandfold Change in Resistivity in Magnetoresistive La-Ca-Mn-O Films. *Science (80-.).* **1994**, *264* (5157), 413–415.

(9) Snyder, G. J.; Hiskes, R.; Di Carolis, S.; Beasley, M. R.; Geballe, T. H. Intrinsic Electrical Transport and Magnetic Properties of La0.67Ca0.33MnO3 and La0.67Sr0.33MnO3 MOCVD Thin Films and Bulk Material. *Phys. Rev. B* **1996**, *53* (21), 14434.

(10) Hwang, H. Y.; Cheong, S.-W.; Ong, N. P.; Batlogg, B. Spin-Polarized Intergrain Tunneling in La2/3Sr1/3MnO3. *Phys. Rev. Lett.* **1996**, *77* (10), 2041–2044.

(11) Chen, A.; Bi, Z.; Tsai, C. F.; Lee, J.; Su, Q.; Zhang, X.; Jia, Q.; Mac Manus-Driscoll, J. L.; Wang, H. Tunable Low-Field Magnetoresistance in (La0.7Sr0.3MnO3)0.5:(ZnO)0.5 Self-Assembled Vertically Aligned Nanocomposite Thin Films. *Adv. Funct. Mater.* **2011**, *21* (13), 2423–2429.

(12) MacManus-Driscoll, J. L.; Zerrer, P.; Wang, H.; Yang, H.; Yoon, J.; Fouchet, A.; Yu, R.; Blamire, M. G.; Jia, Q. Strain Control and Spontaneous Phase Ordering in Vertical Nanocomposite Heteroepitaxial Thin Films. *Nat. Mater.* **2008**, *7*

(4), 314–320.
(13) Dekkers, M.; Nguyen, M. D.; Steenwelle, R.; te Riele, P. M.; Blank, D. H. A.; Rijnders, G. Ferroelectric Properties of Epitaxial Pb(Zr,Ti)O3 Thin Films on Silicon by Control of Crystal Orientation. *Appl. Phys. Lett.* **2009**, *95* (1), 12902.
(14) Mahmoud, A.; Ferrari, A.; Maschio, L.; Sgroi, M. F.; Pullini, D. Ab Initio Simulation of ZnO/LaMnO3 Heterojunctions: Insights into Their Structural and Electronic Properties. *Submitt. to J. Phys. Chem. C*.
(15) Dovesi, R.; Orlando, R.; Civalleri, B.; Roetti, C.; Saunders, V. R.; Zicovich-Wilson, C. M. CRYSTAL: A Computational Tool for the Ab Initio Study of the Electronic Properties of Crystals. *Z. Krist.* **2005**, *220*, 571–573.
(16) Dovesi, R.; Orlando, R.; Erba, A.; Zicovich-Wilson, C. M.; Civalleri, B.; Casassa, S.; Maschio, L.; Ferrabone, M.; De La Pierre, M.; D'Arco, P.; Noël, Y.; Causà, M.; Rérat, M.; Kirtman, B. CRYSTAL14: A Program for the Ab Initio Investigation of Crystalline Solids. *Int. J. Quantum Chem.* **2014**, *114* (19), 1287–1317.
(17) Broyden, C. G. The Convergence of a Class of Double-Rank Minimization Algorithms 1. General Considerations. *J. Inst. Math. Appl.* **1970**, *6*, 76–90.
(18) Civalleri, B.; D'Arco, P.; Orlando, R.; V. R. Saunders, R. D. Hartree-Fock Geometry Optimisation of Periodic Systems with the CRYSTAL Code. *Chem. Phys. Lett.* **2001**, *348*, 131.
(19) Fletcher, R. A New Approach to Variable Metric Algorithms. *Comput. J* **1970**, *13*, 317–322.
(20) Shanno, D. F. Conditioning of Quasi-Newton Methods for Function Minimization. *Math. Comput.* **1970**, *24*, 647–656.
(21) Goldfarb, D. A Family of Variable-Metric Methods Derived by Variational Means. *Math. Comput.* **1970**, *24*, 23–26.
(22) Perdew, J. P.; Burke, K.; Ernzerhof, M. Generalized Gradient Approximation Made Simple. *Phys. Rev. Lett.* **1996**, *77*, 3865.
(23) Hay, P. J.; Wadt, W. R. Ab Initio Effective Core Potentials for Molecular Calculations. Potentials for K to Au Including the Outermost Core Orbitals. *J. Chem. Phys.* **1985**, *82*, 299.
(24) Hay, P. J.; Wadt, W. R. Ab Initio Effective Core Potentials for Molecular Calculations. Potentials for the Transition Metal Atoms Sc to Hg. *J. Chem. Phys.* **1985**, *82*, 270.
(25) Hay, P. J.; Wadt, W. R. Ab Initio Effective Core Potentials for Molecular Calculations. Potentials for Main Group Elements Na to Bi. *J. Chem. Phys.* **1985**, *82*, 284.
(26) Hirshfeld, F. L. Bonded-Atom Fragments for Describing Molecular Charge Densities. *Theor. Chim. Acta* **1977**, *44*, 129.
(27) Adamo, C.; Barone, V. Toward Reliable Density Functional Methods without Adjustable Parameters: The PBE0 Model. *J. Chem. Phys.* **1999**, *110* (13), 6158.
(28) Lee, Y. L.; Kleis, J.; Rossmeisl, J.; Morgan, D. Ab Initio Energetics of LaBO3 (001) (B=Mn, Fe, Co, and Ni) for Solid Oxide Fuel Cell Cathodes. *Phys. Rev. B* **2009**, *80* (22), 224101.
(29) Mastrikov, Y. A.; Merkle, R.; Heifets, E.; Kotomin, E. A.; Maier, J. Pathways for Oxygen Incorporation in Mixed Conducting Perovskites: A DFT-Based Mechanistic Analysis for (La, Sr)MnO3−δ. *J. Phys. Chem. C* **2010**, *114* (7), 3017–3027.
(30) Pavone, M.; Muñoz-García, A. B.; Ritzmann, A. M.; Carter, E. A. First-Principles Study of Lanthanum Strontium Manganite: Insights into Electronic Structure and Oxygen Vacancy Formation. *J. Phys. Chem. C* **2014**, *118* (25), 13346–13356.
(31) Pavone, M.; Ritzmann, A. M.; Carter, E. A. Quantum-Mechanics-Based Design Principles for Solid Oxide Fuel Cell Cathode Materials. *Energy Environ. Sci.* **2011**, *4* (12), 4933.
(32) Van Aert, S.; Verbeeck, J.; Erni, R.; Bals, S.; Luysberg, M.; Dyck, D. Van; Tendeloo, G. Van. Quantitative Atomic Resolution Mapping Using High-Angle Annular Dark Field Scanning Transmission Electron Microscopy. *Ultramicroscopy* **2009**, *109* (10), 1236–1244.
(33) Van Aert, S.; Batenburg, K. J.; Rossell, M. D.; Erni, R.; Van Tendeloo, G. Three-Dimensional Atomic Imaging of Crystalline Nanoparticles. *Nature* **2011**, *470* (7334), 374–377.
(34) De Backer, A.; van den Bos, K. H. W.; Van den Broek, W.; Sijbers, J.; Van Aert, S. StatSTEM: An Efficient Approach for Accurate and Precise Model-Based Quantification of Atomic Resolution Electron Microscopy Images. *Ultramicroscopy* **2016**, *171*, 104–116.
(35) Martin, M. C.; Shirane, G. Magnetism and Structural Distortion in the La0.7Sr0.3MnO3 Metallic Ferromagnet. *Phys. Rev. B* **1996**, *53* (21), 285–290.
(36) Morkoç, H.; Özgür, Ü. *Zinc Oxide: Fundamentals, Materials and Device Technology*; Wiley, 2008.
(37) Mulliken, R. S. Electronic Population Analysis on LCAO-MO Molecular Wave Functions. I. *J. Chem. Phys.* **1955**, *23* (10), 1833.

Experimental HAADF-STEM image with superimposed the structural model used in DFT calculations. Scale bar is 5Å.